

NUMERICAL ANALYSIS OF THE EFFECT OF HEAT INPUT IN THE SPOT WELDING OF DISSIMILAR MATERIALS

NUMERIČNA ANALIZA VNOSA TOPLOTE PRI TOČKOVNEM VARJENJU DVEH RAZLIČNIH MATERIALOV

M. Vigneshkumar^{1*}, P. Ashoka Varthanan¹, S. Senthil Murugan²,
G. Gokilakrishnan³

¹Department of Mechanical Engineering, Sri Krishna College of Engineering and Technology, Coimbatore, India

²Department of Mechanical Engineering, Rajalakshmi Engineering College, Chennai, India

³Department of Mechanical Engineering, Sri Eshwar College of Engineering, Coimbatore, India

Prejem rokopisa – received: 2022-02-17; sprejem za objavo – accepted for publication: 2022-04-28

doi:10.17222/mit.2022.411

Resistance spot welding (RSW) of dissimilar metals is an emerging trend in automobile industries in the manufacture of passenger-vehicle bodies. It provides the material characteristics and advantages of both metals. In this research work, the influence of heat addition and maximum interface temperature in the RSW of austenitic stainless-steel sheets (AISI 304 and AISI 316L) is investigated by welding the specimens at various levels of welding current and weld time. The ultimate strength of the spot-welded joints is analyzed to evaluate the amount of heat utilization and the quality of spot welds, finite-element analysis, and macrostructural evaluations. The thermal distribution profile and stress-strain analysis on the welded specimens are carried out with the 3D finite-element model developed using ABAQUS V6.6 software through incremental electro-thermal-structural analysis. A maximum tensile shear failure strength of 253 MPa was obtained with a nugget diameter 6.55 mm and the heat utilization being 59.69 %.

Keywords: resistance spot welding, numerical analysis, heat utilization, nugget growth, Schaeffler diagram

Razvoj novih metod uporovnega točkovnega varjenja (RSW; angl.: Resistance Spot Welding) različnih oziroma nekompatibilnih materialov je postal trend v avtomobilski industriji in proizvodnji ohišij drugih vrst transportnih vozil. To naj bi zagotavljalo in ohranjalo lastnosti in prednosti obeh medsebojno zvarjenih kovin. V pričujočem članku avtorji opisujejo raziskavo vpliva vnosa toplote in maksimalne temperature na meji med izbranimi zvarjenima kovinama. V eksperimentalni raziskavi so izbrali za medsebojno točkovno varjenje pločevini iz avstenitnega nerjavnega jekla AISI 304 in AISI 316L. Preizkuse varjenja na izbranih vzorcih so izvajali pri različnih nivojih in časih električnega toka varjenja. Maksimalno porušno trdnost točkovno zvarjenih spojev so analizirali in ovrednotili glede na količino vnešene energije (toplote) in kakovosti nastalih točkovnih zvarov s pomočjo metode končnih elementov in makrostrukturnega ocenjevanja. Profil porazdelitve toplote in napetostno-deformacijsko analizo zvarjenih vzorcev so določili s pomočjo modela na osnovi 3-D metode končnih elementov. Za to so uporabili programsko orodje ABAQUS V6.6 in metodo inkrementalno elektro-termične strukturne analize. Maksimalna strižno-natezna porušitev zvarnega spoja je nastopila pri 253 MPa in njegovem premeru 6,55 mm ob 59,69 % izkoristku toplote.

Ključne besede: uporovno točkovno varjenje, numerična analiza, toplotni izkoristek, rast zvarne leče, Schaefflerjev diagram

1 INTRODUCTION

The resistance spot welding process (RSW) has been widely involved in the production of cars, buses, trucks, and railway bodies. The RSW process's importance is emphasized by the fact that each car assembly consists of approximately 5000 to 7000 spot welds.¹

The RSW process's significant advantages are that it is fast, well suited for high volume production, and easily automated.² The automobile industries' focus is shifted towards manufacturing lightweight passenger vehicles at low cost with enhanced features such as reliability and build quality.³ The desired characteristics cannot be met with an individual metal, and there comes the need to join different metals.⁴ However, at the same time, it is impossible to spot weld materials with a vast difference in material properties such as melting point, ther-

mal, and electrical conductivity. Nugget offset was observed when welding most dissimilar metals due to the heat imbalance caused by the differences in the material properties of both metals.⁵⁻⁷ It deteriorates the mechanical performance of welded joints and limits its practical applications. The AISI 304/316L structure can be used in an automobile chassis with the external surfaces shall be AISI 316L to have better corrosion resistance. AISI 304 can be used for the internal surfaces to reduce the cost of the structure.

2 EXPERIMENTAL PART

The finite-element modeling of RSW is challenging since it requires simultaneous physical electrical-thermal interaction.⁸ Feulvarch et al.⁹ analyzed two finite-element models for establishing the necessary boundary conditions in the RSW process. The model assumed normal flux transfer between two elements as they were close to

*Corresponding author's e-mail:
vigneshkumarmech@gmail.com (M. Vigneshkumar)

Table 1: Heat utilization in the RSW of dissimilar sheets

Sl. No.	Welding current (kA)	Number of welding cycles	Nugget volume (mm ³)	Average resistance value ($\mu\Omega$)	Heat input (J)	Heat utilized (J)	Heat utilized (%)	Ultimate stress – FEA model (MPa)	Actual ultimate stress (MPa)
1.	6	4	16.78	89.20	256.91	95.18	37.05	176.1	183
2.	6	6	25.82	87.61	378.47	157.45	41.60	186.8	196
3.	6	8	31.47	86.35	497.37	203.87	40.99	192.4	195
4.	6	9	35.58	85.85	556.30	236.41	42.50	204.6	212
5.	6	10	38.15	85.46	615.31	258.78	42.06	210.6	211
6.	7	4	28.87	86.58	339.39	184.93	54.49	180.2	185
7.	7	6	38.09	84.66	497.80	270.09	54.26	188.7	193
8.	7	8	42.18	83.54	654.95	321.46	49.08	218.6	222
9.	7	9	51.35	83.17	733.55	402.54	54.88	216.4	218
10.	7	10	57.00	82.89	812.32	457.31	56.30	233	235
11.	8	4	32.99	83.99	430.02	243.75	56.68	190.4	195
12.	8	6	48.22	82.54	633.90	401.03	63.26	198.6	207
13.	8	8	50.90	82.07	840.39	458.30	54.53	235.6	239
14.	8	9	46.62	82.04	945.10	432.09	45.72	241.9	248
15.	8	10	58.52	82.06	1050.36	555.14	52.85	243.7	246
16.	9	4	43.82	82.31	533.36	375.00	70.31	212.4	220
17.	9	6	50.90	82.17	798.69	496.43	62.16	238.6	244
18.	9	8	60.45	83.01	1075.81	640.09	59.50	242.4	248
19.	9	9	66.68	83.52	1217.72	726.90	59.69	248.4	253
20.	9	10	60.09	84.04	1361.44	670.93	49.28	240.7	248

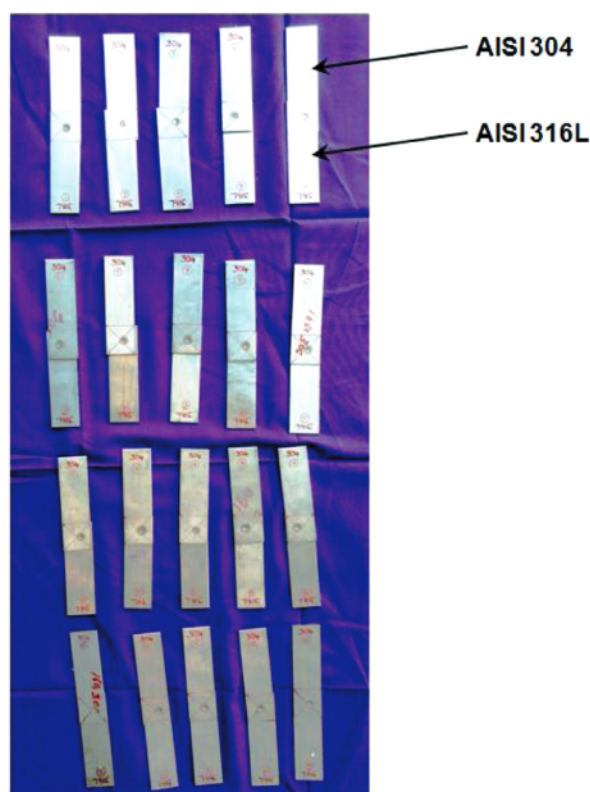
each other. The second model considered the relative displacements between the contact elements in establishing the contact conditions, thus providing better results than the previous model. However, the mechanical contact area was not considered to establish the thermal contact conditions, and it was selected arbitrarily. Vignesh et al.¹⁰ attempted to join AISI 316L and duplex sheets using a spot-welding process. They found that the developed finite-element model predicted the maximum failure stress value of 660.32 MPa with 0.1 % of error.

Based on a literature survey it is found that in most cases the nugget growth is correlated with welding current, the diameter of the electrode, and weld time for spot welding of similar metals based on a numerical analysis using a mechanical-thermal-electrical coupled model.^{11–13} However, the influence of heat input on the nugget's growth and the percentage of heat being utilized in the joining of similar or dissimilar metals using RSW are not explored, to the best of our knowledge. Hence, in this research work, an extensive investigation of the influence of heat input and the percentage heat utilized in the formation of weld nugget for the spot welding of dissimilar austenitic steel sheets is analyzed using the commercial finite-element software Abaqus 6.11.

AISI 304 sheet of 1.5 mm thickness and AISI 316L sheet of 2 mm thickness are cut into the required size of 30 mm × 30 mm, as per the AWS D8.9-97 standard using a shearing machine,² as shown in **Figure 1**.

Specimens are cleaned with acetone to remove the dirt and rust present and welded using a 35 kVA AC spot welder JPC 35. Trial experiments are initially conducted with constant welding current with varying welding time and vice versa to arrive at the practical process parameter

levels for the selected dissimilar material and its thickness. Based on trial experiments, a full factorial design of experiments is developed with the welding current varied between 6 kA and 9 kA and 4–10 welding cycles, as presented in **Table 1**.

**Figure 1:** Resistance spot welded dissimilar specimens

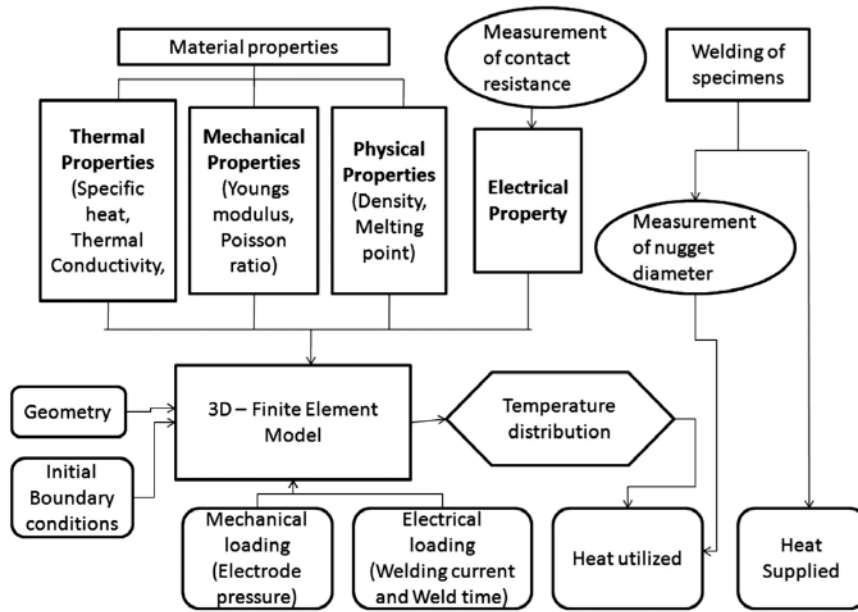


Figure 2: Flowchart depicting the methodology of the analysis

The holding time, squeeze time, and electrode pressure are maintained at 10 welding cycles, 12 welding cycles, and 1.5 bar, respectively. The methodology adopted for evaluating the heat input on the spot-welded nugget's quality is depicted in Figure 2. Microstructural images are captured by Carl Zeiss type optical microscope to study the phase transformations in the weld nugget. The microhardness test is performed to evaluate the welded joints' plastic and elastic behaviors by conducting hardness tests at several locations, such as the nugget area, heat-affected area, and base metals using a Vickers hardness test. It is performed in the transverse direction from the top specimen of AISI 316L to the bottom specimen of AISI 304 across the weld nugget. The time duration between the application of the force from the beginning to 9.8 N is achieved in 10 s. For all the indentations, the approach velocity is maintained at 150 μm/s.

The finite-element model is subjected to a convergence test after meshing to reduce the computation time in the stress-strain analysis.¹⁴ All the active edges at the end of the AISI 316L side are fixed using the ABAQUS software's encastre boundary condition. Both the translation (U1 = 0, U2 = 0 and U3 = 0) and rotation motion (UR1 = UR2 = UR3 = 0) are restricted in all directions. The AISI 304 plate is loaded as well as permitted to move in the linear direction (U2 = U3 = 0 and UR1 = UR2 = UR3 = 0). Fine mesh is used at the contact surfaces of the electrode and workpiece and a course mesh is used at the remaining sections to reduce the computation time. The Q3D8 element of the Abaqus software with 5 degrees of freedom and a total of 30026 nodes is used in the current model. Numerical simulations are performed on the finite-element model by applying a load on the AISI 304 specimen in the x direction until

the nugget is pulled out from the specimen, and the results are evaluated.

The standard Johnson Cook material parameters for AISI 304 and AISI 316L are obtained from the experimental quasi-static uniaxial tensile tests performed at varying strain rates and temperatures, as shown in Table 2.¹⁵⁻¹⁷ The Coefficients of A, B, C, n, and m are acquired to fit the Johnson Cook empirical model to determine the strain rate, as shown in Equation (1).¹⁰

$$\delta_{eq} = (A + B\epsilon_{eq}^n)(1 + C \ln(\epsilon_{eq}^*)) (1 - T^{*m}) \quad (1)$$

δ_{eq} , ϵ_{eq}^* and T^{*m} are the equivalent stress, equivalent plastic strain, and triaxility, respectively.

The material parameter A is taken as 0.2 % of the off-set yield stress at ambient temperature. The B and n parameter values are selected for the curve fitting, C from the high strain experimental analysis conducted at ambient temperature, and m from the high-temperature test data.

$$\epsilon_f^{JC} = (D_1 + D_2 \exp(D_3 \sigma^*)) (1 + D_4 \ln \epsilon_{eq}^*) (1 + D_5 T^*) \quad (2)$$

whereas D_1 , D_2 , D_3 , D_4 , D_5 are the material constants, T^* and σ^* represent the homologous temperature and triaxility, respectively.

The Jonson-Cook material damage parameters for the AISI 304 sheet used in the Abaqus explicit software for simulation are as follows: $D_1 = 0.69$, $D_2 = D_3 = D_5 = 0$, $D_4 = 0.0546$.^{18,19} The corresponding values for the AISI 316L sheets are $D_1 = 0.05$, $D_2 = 3.44$, $D_3 = 2.12$, $D_5 = 0$, $D_4 = 0.002$.¹⁰

$$T^* = (T - T_r) / (T_m - T_r) \quad (3)$$

T_m , T , and T_r are the temperatures of the different conditions such as melting, ambient, and absolute, respectively.

$$\omega = (\epsilon_{eq}^0 + \sum \Delta \epsilon_{eq}) / \epsilon_f^{JC} \quad (4)$$

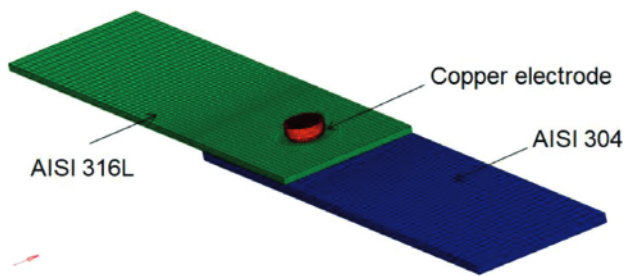


Figure 3: Numerical model to evaluate thermal distribution and strain analysis in RSW process

where ω is the damage parameter, ϵ^0_{eq} is the initial plastic strain, ϵ_{eq} is the incremental equivalent plastic strain. The model predicts the nodal point value of the equivalent plastic strain, and it is assumed that failure occurs if $\omega > 1$ occurs. The model can predict the high strain rate of metals, and hence it is suitable for testing the integrity of spot-welded sheets.

Table 2: Standard material parameter value for Johnson Cook failure model

	A (MPa)	B (MPa)	n	C	m	ϵ_f^{JC}
AISI 316L	238	1202.4	0.675	0.0224	1.083	0.49
AISI 304	280	802.5	0.622	0.0799	1	1

3 RESULTS AND DISCUSSION

The outcomes of the numerical and experimental investigations are shown in Table 2. The developed 3D numerical model is shown in Figure 3. From the results, the diameter of the weld nugget can be inferred as directly proportional to the heat input. The heat input tends to increase as the welding current and welding time increase. At a welding current of 6 kA and 4 welding cycles, heat input amounts to 256.91 J. The nugget diameter is found to be 4.82 mm, which is just 68.8 % of the electrode diameter, equal to 7 mm. It indicates inadequate heat input and produces a nugget volume of 16.78 mm³. The ultimate strength is relatively low and observed to be 183 MPa. Also, the maximum interface

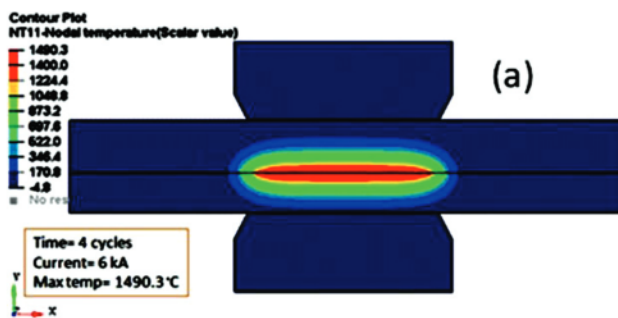


Figure 4: Temperature gradient profile for 6 kA welding current and 4 cycles time

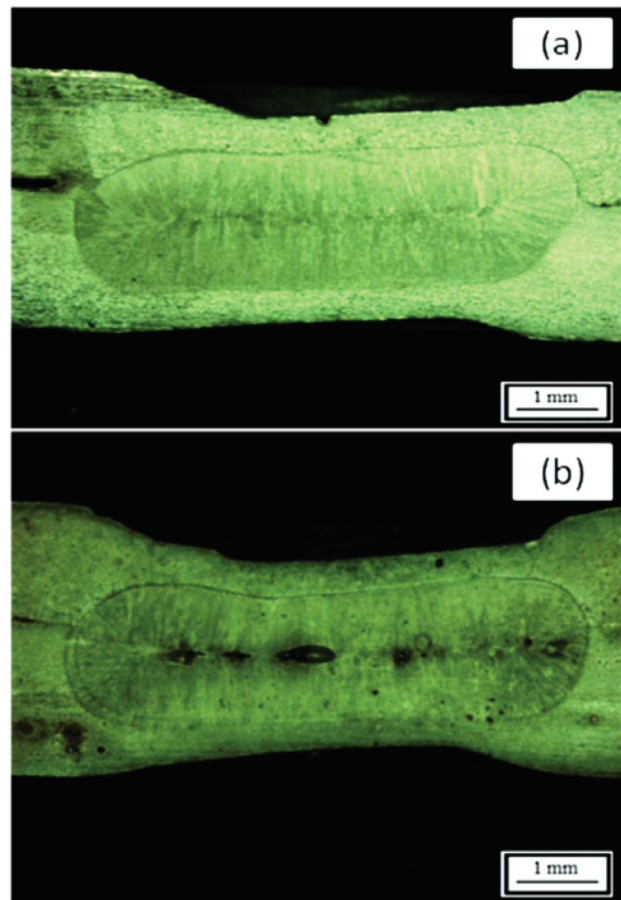


Figure 5: Macrostructure samples: a) sound spot weld, b) defective spot weld

temperature is 1490.3 °C, as shown in Figure 4, which is just above the melting point of both the materials.

The optimal nugget diameter for the maximum ultimate strength of 253 MPa is obtained with a heat input of 1217.72 J when the current of 9 kA is passed for 9 welding cycles.

The nugget volume was found to become the maximum of 66.68 mm³ with an interface temperature of 2836.2 °C. The nugget diameter obtained (6.55 mm) is 93.57 % of the electrode diameter, with the heat utilization being 59.69 %. The welded specimen's macrostructure indicates the nugget is free of voids, as shown in Figure 5a. The maximum heat input of 1361.44 J when the 9 kA welding current is passed for a period of 10 welding cycles causing an increase of nugget diameter (6.73 mm), but a decrease of the nugget thickness (1.69 mm), leading to a decrease in the nugget volume to 60.09 mm³. The weld nugget's ultimate strength is reduced to 248 MPa on account of a smaller nugget volume and the ejection of the base-metal melt from the interface because of overheating. It is verified by the existence of a void in the weld nugget of specimen 20, as shown in Figure 5b.

The lowest ultimate stress of the welded joint is attributed to an insufficient heat input. The ultimate stress

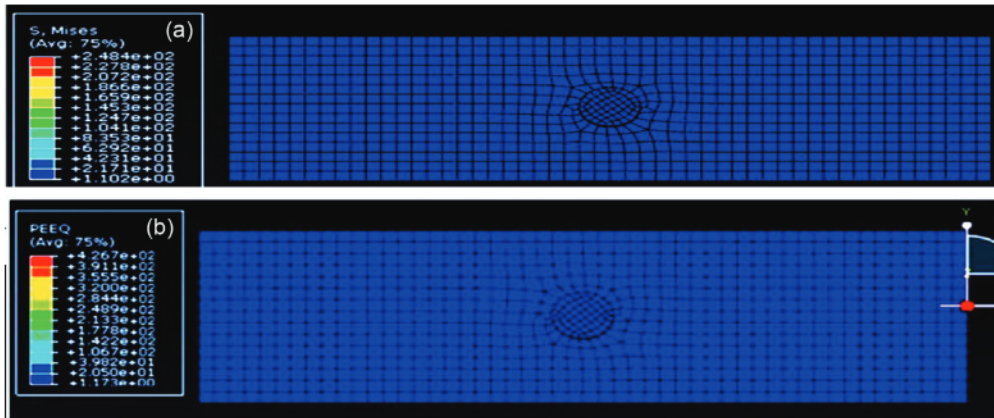


Figure 6: FEA-based highest tensile shear failure load: a) ultimate stress and b) strain

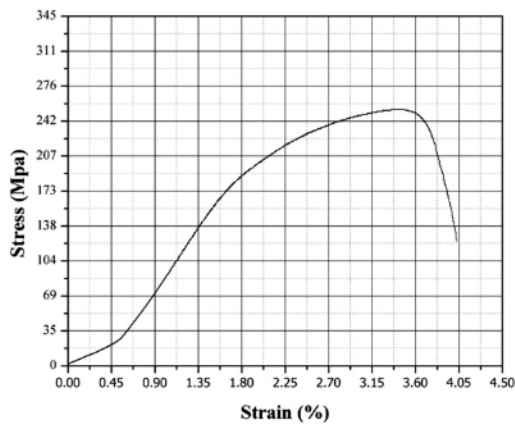


Figure 7: Experimental ultimate stress and strain for the highest tensile shear failure load

increases with the increase of the heat input. The subsequent increase of the welding current to 7 kA, 8 kA, and 9 kA at 10 welding cycles, the ultimate stress is found to be 233 MPa, 243.7 MPa, and 240.7 MPa, respectively.

The maximum ultimate stress of 248.4 MPa with a plastic strain of 4.267% is observed in trial 19, as presented in **Figure 6a** and **6b**, respectively. The experimental ultimate stress and strain for trial 19 is 253 MPa and 4.46 % strain, as shown in **Figure 7**. It shows that the numerical model exhibits a better similarity with the experimental model and the error percentage being just 2.26 %.

The weld-nugget microstructure obtained for specimen 19 using the electron microscope is shown in **Figure 8**. The base-metal AISI 304, AISI 316L, and the weld nugget are indicated in **Figure 8a**.

As the interface temperature is much higher than the alloying elements' solidus temperature in the austenitic stainless steel, alloying elements are melted in the heat-affected and fusion zone. Thus, it leads to the formation of a supersaturated austenite solution on cooling with the delta ferrite (δ) precipitation in the austenite matrix. The existence of δ -ferrite in the nugget zone is shown in **Figure 8b**. The amount of δ -ferrite in the area adjacent to the heat-affected-zone boundary is more than at the center of the weld nugget. It is evident that the so-

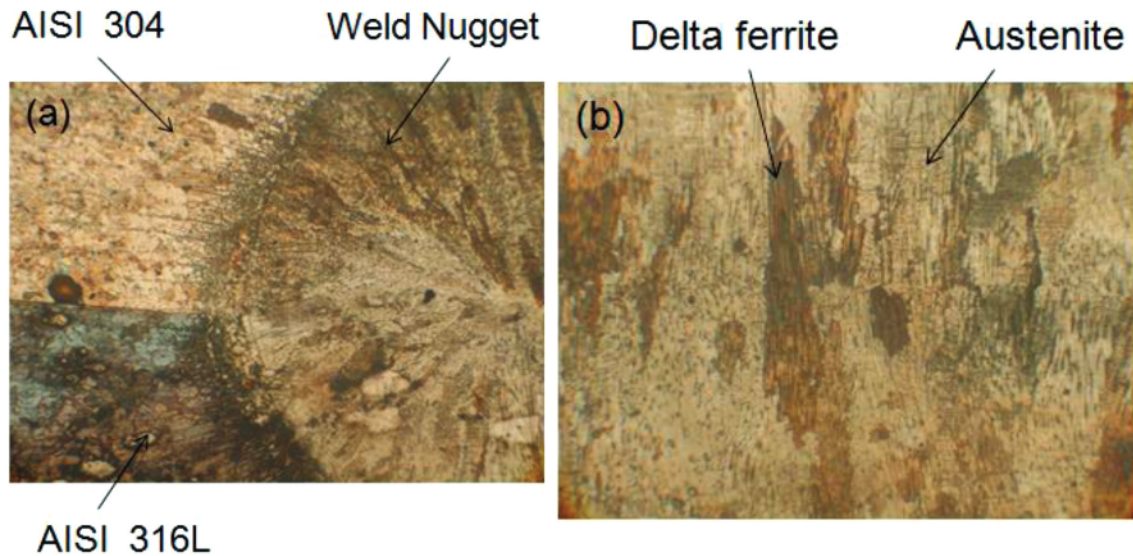


Figure 8: Spot-weld microstructure: a) weld nugget, b) delta ferrite and austenite

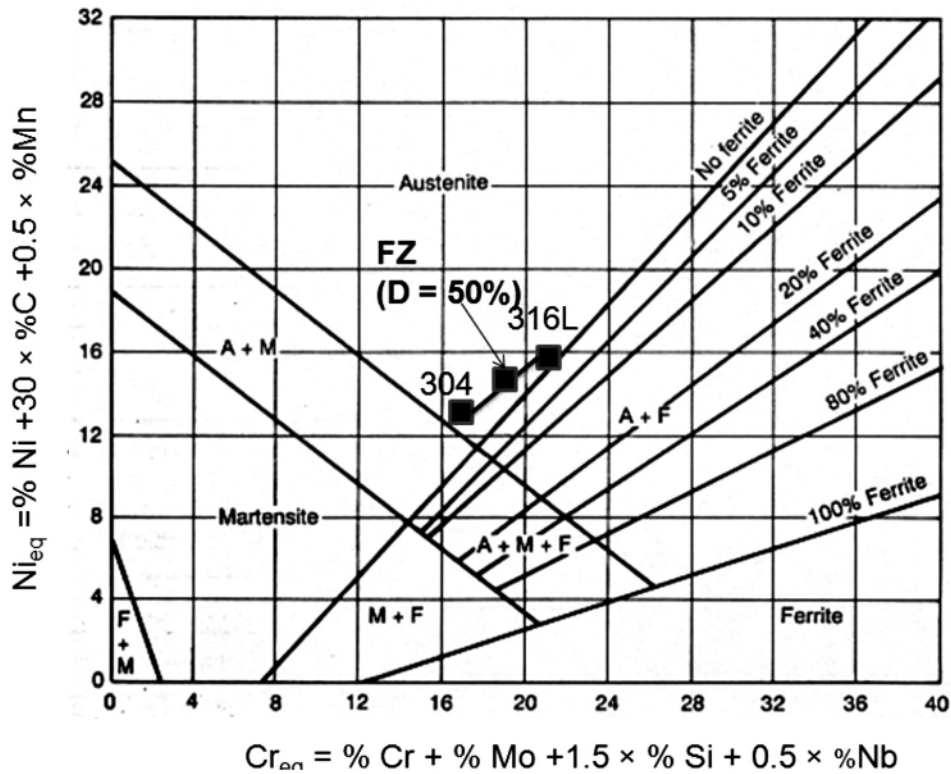


Figure 9: Prediction of weld nugget's microstructure with Schaeffler diagram

lidification occurred in the ferrite austenite mode (FA). The cooling rate at the interior of the fusion zone is smaller compared to the boundary due to the presence of water-cooled electrodes. Hence, the austenite dissolves ferrite at the interior of the fusion zone due to the lower cooling rate. However, the absorption of ferrite by the austenite at the boundary is prevented by rapid cooling. The Schaeffler diagram can be used to estimate the weld nugget's microstructure based on the equivalent chromium and nickel contents in the base metal.²⁰⁻²³ The chromium and nickel equivalents for the AISI 304 are 17.125 and 13.4, respectively, whereas, for AISI 316L, it is 20.5 and 15.9. The equivalent composition indicates both the base metals' microstructure to be fully austenitic, as shown in Figure 9.

It has been found that the centerline of the weld nugget coincides with the base-metal interface. It is highly desired for better mechanical strength, and it is attributed to the identical material properties of both the materials.²⁴ The dilution ratio is the proportion of each base metal in the weld nugget. For the dilution ratio of 50 %, the resultant weld structure must be fully austenitic as per the Schaeffler diagram. The deviation between the actual and predicted microstructure could be due to the accelerated high cooling rate induced by the water-cooled electrodes used in the process. The cooling rate of the RSW process is more than 1000 °C.²⁴ The weld's microstructure is free of any intergranular crack in the heat-affected zone and void on account of excess heat input, indicating a sound weld joint. The thermal ef-

iciency of the spot-welding process (70.31 %) is observed to be less than an arc-welding process (79.5 %).²⁵

4 CONCLUSIONS

In the present work, the influence of heat input and maximum interface temperature on nugget volume in the RSW of stainless steel (AISI 304 and 316L) is studied using a 3D finite-element model, and the following observations are made:

- The minimum heat required for nugget formation for the RSW process of the selected dissimilar sheets is found to be 256.91 J., But the tensile shear failure load is observed to be a minimum of 7.85 kN, and only 37.05 % of the heat input is utilized.
- The nugget diameter and the nugget volume are generally found to be increasing with heat input until overheating of the specimens causes expulsion.
- The optimal heat input of 1217.72 J delivers the highest tensile shear failure load, with 59.69 % of the heat utilized. The microstructure of the specimen also indicates the efficient joining of dissimilar austenitic stainless steels with a defect-free weld nugget.
- The excessive heat of 1361.44 J causes increases in the nugget diameter, but a decrease in the nugget thickness, leading to an overall reduction in the nugget's volume. The excessive heat causes voids in the weld nugget, leading to the poor mechanical performance of the spot-welded specimens.

5 REFERENCES

- ¹ H. Zhang, X. Qiu, F. Xing, B. Jie, J. Chen, Failure analysis of dissimilar thickness resistance spot welded joints in dual-phase steels during tensile shear test, *Mater. Des.*, 55 (2014), 366–372, doi:10.1016/j.matdes.2013.09.040
- ² T. Jagadeesha, T. J. Sarvoththama Jothi, Studies on the influence of process parameters on the AISI 316L resistance spot-welded specimens, *Int J Adv Manuf Tech.*, 93 (2017) 1–4, 73–88, doi:10.1007/s00170-015-7693-y
- ³ M. Tamizi, M. Pouranvari, M. Movahedi, Welding metallurgy of martensitic advanced high strength steels during resistance spot welding, *Sci. Technol. Weld. Joining*, 22 (2017) 4, 327–335, doi:10.1080/13621718.2016.1240979
- ⁴ X. Luo, J. Ren, D. Li, Y. Qin, P. Xu, Macro characteristics of dissimilar high strength steel resistance spot welding joint, *Int. J. Adv. Manuf. Tech.*, 87 (2016) 1–4, 1105–1113, doi:10.1007/s00170-016-8581-9
- ⁵ J. Wang, H. Wang, F. Lu, B. Carlson, D. Sigler, Analysis of Al-steel resistance spot welding process by developing a fully coupled multi-physics simulation model, *Int. J. Heat. Mass. Tran.*, 89 (2015), 1061–1072, doi:10.1016/j.ijheatmasstransfer.2015.05.086
- ⁶ M. Vigneshkumar, P. Ashoka Varthanan, Comparison of RSM and ANN model in the prediction of the tensile shear failure load of spot welded AISI 304/316 L dissimilar sheets, *Int. J. Comput. Mater. Sci. Surf. Eng.*, 8 (2019) 2, 114–130, doi:10.1504/IJCMSSE.2019.102292
- ⁷ M. Vigneshkumar, P. Ashoka Varthanan, Y. Maria Ambrose Raj, Finite element-based parametric studies of nugget diameter and temperature distribution in the resistance spot welding of AISI 304 and AISI 316L sheets, *Transactions of the Indian Institute of metals*, 72 (2019) 2, 429–438, doi:10.1007/s12666-018-1494-6
- ⁸ J. E. Gould, An examination of nugget development during spot welding using both experimental and analytical techniques, *Weld J.*, 66 (1987) 1, 01–10
- ⁹ E. Feulvarch, V. Robin, J. M. Bergheau, Resistance spot welding simulation: a general finite element formulation of electro thermal contact conditions, *J. Mater. Process. Technol.*, (2004), 436–441, doi:10.1016/j.jmatprotec.2004.04.096
- ¹⁰ K. Vignesh, A. Elaya Perumal, P. Velmurugan, Resistance spot welding of AISI-316L SS and 2205 DSS for predicting parametric influences on weld strength – Experimental and FEM approach, *Archives of civil and mechanical engineering*, 19 (2019) 4, 1029–1042, doi:10.1016/j.acme.2019.05.002
- ¹¹ Z. Hou, I. Kim, Y. Wang, C. Li, C. Chen, Finite element analysis for the mechanical features of resistance spot welding process, *J. Mater. Process. Technol.*, 185 (2007), 160–165, doi:10.1016/j.jmatprotec.2006.03.143
- ¹² B. Wang, L. Hua, X. Wang, Y. Song, Y. Liu, Effects of electrode tip morphology on resistance spot welding quality of DP590 dual-phase steel, *Int. J. Adv. Manuf. Tech.*, 83 (2016) 9–12, 1917–1926, doi:10.1007/s00170-015-7703-0
- ¹³ H. Moshayedi, I. Sattari-far, Numerical and experimental study of nugget size growth in resistance spot welding of austenitic stainless steels, *J. Mater. Process. Tech.*, 212 (2012), 347–354, doi:10.1016/j.jmatprotec.2011.09.004
- ¹⁴ T. Chino, A. Kunugi, T. Kawashima, G. Watanabe, C. Can, N. Ma, N. Fast, Prediction for resistance spot welding deformation using inherent strain method and nugget model, *Materials*, 14 (2021), 7180, doi:10.3390/ma14237180
- ¹⁵ J. Qiang Tan, M. Zhan, S. Liu, T. Huang, J. Guo, H. Yang, A modified Johnson–Cook model for tensile flow behaviors of 7050-T7451 aluminum alloy at high strain rates, *Materials Science and Engineering: A*, 631 (2015), 214–219, doi:10.1016/j.msea.2015.02.010
- ¹⁶ A. Banerjee, S. Dhar, S. Acharyya, D. Datta, N. Nayak, Determination of Johnson Cook material and failure model constants and numerical modelling of Charpy impact test of armour steel, *Materials Science and Engineering A*, 640 (2015), 200–209, doi:10.1016/j.msea.2015.05.073
- ¹⁷ H. K. Farahani, M. Ketabchi, S. Zangeneh, Determination of Johnson–Cook Plasticity Model Parameters for Inconel718, *J. of Mater. Eng. and Perform.*, 26 (2017), 5284–5293, doi:10.1007/s11665-017-2990-2
- ¹⁸ E. A. Flores-Johnson, O. Muransky, C. J. Hamelin, P. J. Bendeich, L. Edwards, Numerical analysis of the effect of weld-induced residual stress and plastic damage on the ballistic performance of welded steel plate, *Comput. Mater. Sci.*, 58 (2012), 131–139, doi:10.1016/j.commatsci.2012.02.009
- ¹⁹ P. Krasauskas, S. Kilikevicius, R. Cesnavicius, D. Pacenga, Experimental analysis and numerical simulation of the stainless AISI 304 steel friction drilling process, *Mechanika*, 20 (2014) 6, 590–595, doi:10.5755/j01.mech.20.6.8664
- ²⁰ B. Wittig, M. Zinke, S. Jüttner, A new constitution diagram for dissimilar metal welds of high-manganese steels, *Weld World*, 63 (2019), 491–499, doi:10.1007/s40194-018-0668-5
- ²¹ R. Othman, T. Dorin, N. Stanford, P. Hodgson, The microstructure of high manganese TWIP steels produced via simulated direct strip casting, *Materials Science and Technology*, 38 (2022) 1, 30–38, doi:10.1080/02670836.2021.2021501
- ²² Z. Liu, C. Fan, C. Chen, Z. Ming, C. Yang, S. Lin, L. Wang, Design and evaluation of nitrogen-rich welding wires for high nitrogen stainless steel, *Journal of Materials Processing Technology*, 288 (2021), 116885, doi:10.1016/j.jmatprotec.2020.116885
- ²³ P. Marashi, M. Pouranvari, S. Amirabdollahian, A. Abedi, M. Goodarzi, Microstructure and failure behaviour of dissimilar resistance spot welds between low carbon galvanized and austenitic stainless steels, *Mat. Sci. Eng. A, Struct.*, 480 (2008) 1–2, 175–180, doi:10.1016/j.msea.2007.07.007
- ²⁴ T. C. A. Colombo, R. R. Rego, J. Otubo, A. R. de Faria, Mechanical reliability of TWIP steel spot weldings, *Journal of Materials Processing Technology*, 266 (2019), 662–674, doi:10.1016/j.jmatprotec.2018.11.021
- ²⁵ R. M. Farias, P. R. F. Teixeira, L. O. Vilarinho, An efficient computational approach for heat source optimization in numerical simulations of arc welding processes, *Journal of Constructional Steel Research*, 176 (2021), 106382, doi:10.1016/j.jcsr.2020.106382